

Bose-Einstein Condensation of Potassium Atoms by Sympathetic Cooling

G. Modugno, G. Ferrari, G. Roati, R. J. Brecha, A. Simoni, M. Inguscio

We report on the Bose-Einstein condensation of potassium atoms, whereby quantum degeneracy is achieved by sympathetic cooling with evaporatively cooled rubidium. Because of the rapid thermalization of the two different atoms, the efficiency of the cooling process is high. The ability to achieve condensation by sympathetic cooling with a different species may provide a route to the production of degenerate systems with a larger choice of components.

Since the first realizations of Bose-Einstein condensation (BEC) in a dilute gas of alkali atoms (1–3), research in the interdisciplinary fields of atom optics and quantum fluids has flourished (4). BEC has been observed in five atomic species: H (5), ^4He (6), ^7Li (3), ^{23}Na (2), and the two isotopes ^{85}Rb (7) and ^{87}Rb (1). Direct forced evaporative cooling of the bosonic isotopes of potassium has been prevented by limitations in the temperature and density ranges achievable by laser cooling (8). We show that by taking advantage of thermalization between a small dilute sample of potassium (^{41}K) and evaporatively cooled rubidium (^{87}Rb), these limitations can be overcome. The technique of sympathetic cooling had been proposed for the cooling of ions (9) and, in the case of neutral trapped atoms, has been used to obtain quantum degeneracy, but only for two different internal states of the same atom (10) or for two isotopes of the same species (11–13). The mixing of two different atomic species turned out to be a successful strategy, although their interaction properties could be discovered only by attempting the experiment. In the case of K, sympathetic cooling of its fermionic isotope ^{40}K (14) with Rb represents the natural extension of this technique, and may be a new way to explore the physics below Fermi temperature (15), as demonstrated in the case of Li (12, 16).

The experimental apparatus is based on a conventional double magneto-optical trap (MOT) apparatus, although the complexity is increased because of the requirement for the simultaneous trapping and cooling of two different atomic species. K and Rb atoms are captured from a vapor background in the first MOT (MOT1) and then transferred by resonant laser beams to a second cell with a much lower background pressure, where they are recaptured in a second MOT (MOT2) and

loaded in a magnetic trap. Evaporative cooling of Rb is performed, and the evolution of both samples is monitored by means of absorption imaging.

The laser system to manipulate the two atomic species consists of three sources: a titanium:sapphire laser operating on the K optical transitions (767 nm) and two diode lasers operating on the Rb transitions (780 nm). The two pairs of frequencies at different wavelengths necessary for magneto-optical trapping are then injected simultaneously in a semiconductor tapered amplifier (TA), which provides the required power for the two MOTs (17).

The experimental sequence begins with the loading of Rb in MOT2 for 30 s. During this phase, the TA power is totally dedicated to Rb, and 10^9 Rb atoms are loaded into MOT2. Half of the TA power is then switched to K, and about 10^7 K atoms are loaded into MOT2 in 8 s. The overall efficiency of the Rb MOT in this phase is strongly reduced because of nonlinear processes in the TA, resulting in a loss of about 50% of the initial Rb sample (18).

The magnetic trap consists of a Ioffe-Pritchard potential created by three coils in quadrupole Ioffe configuration (QUIC) (19). Both species are optically pumped into the low-field seeking state $|F = 2, m_F = 2\rangle$, before magnetic trapping. The typical axial and radial oscillation frequencies of Rb in the harmonic trap are $\nu_{\text{ax}} = 16$ Hz and $\nu_{\text{rad}} = 200$ Hz, respectively, whereas those of K are larger by a factor $(M_{\text{Rb}}/M_{\text{K}})^{1/2} = 1.46$, where M_{Rb} and M_{K} are the masses of the two species. In the QUIC, we typically load 2×10^8 Rb atoms and 2×10^6 K atoms, with both at a temperature of about 300 μK .

Evaporative cooling of Rb is done with a microwave knife tuned to the hyperfine transition at 6.8 GHz, which induces transitions from the trapped state to the untrapped $|F = 1, m_F = 1\rangle$ state, without affecting the K sample. Thus, the evaporation reduces the temperature of both trapped samples, in principle keeping the K population constant. Actually, we observe losses of K atoms in the first part of the evaporation, which can be minimized by forcing the speed of the evaporation ramp. We attribute these losses

perature of liquid nitrogen in order to minimize the roughness of the Al surface.

19. Capacitance measurements on two large Al films separated by such an oxide layer indicates a thickness of about 2 nm, whereas ellipsometry measurements indicate a value of about 5 nm.
20. Several volts can be applied to the gate without destroying the oxide layer. This is quite remarkable because the insulator layer is only a few nanometers thick, and it indicates the excellent quality of the gate oxide. The breakdown threshold voltage where the layer is destroyed is typically between 2 and >4 V. A small gate leakage current (a few pA) is observed for V_g approaching such large gate voltages. The whole $I(V_g)$ curve may be somewhat shifted horizontally in a hysteretic way after a sweep to such extreme gate voltages (~ 4 V). For this reason, we refrain from fitting the horizontal position of the $I(V_g)$ curve with the theory that is discussed in the text.
21. P. Horowitz, W. Hill, *The Art of Electronics* (Cambridge Univ. Press, Cambridge, 1980).
22. The data of Fig. 3 can be fitted to a generic p -type metal oxide semiconductor FET (MOSFET) model. The model describes the current in the linear regime as $I = -k(1 - \lambda V_{gs})V_{sd}[2(V_g - V_t) - V_{sd}]$ and the current in the saturation regime as $I = -k(1 - \lambda V_{gs})(V_g - V_t)^2$, with k and λ as fit parameters and V_t the threshold voltage. These equations were found to approximate the data well for the parameters $k = 2.3 \times 10^{-7}$ A/V 2 , $V_t = -1$ V, and $\lambda = 1$ V $^{-1}$. This model provides a reasonable starting point for modeling our devices, but a full theoretical description will need to consider the one-dimensional nature and semi-ballistic transport of semiconducting carbon nanotubes.
23. C. Zhou, J. Kong, H. Dai, *Appl. Phys. Lett.* **76**, 1597 (2000).
24. C. P. Collier *et al.*, *Science* **285**, 391 (1999).
25. A. A. Odintsov, *Phys. Rev. Lett.* **85**, 150 (2000).
26. F. Léonard, J. Tersoff, *Phys. Rev. Lett.* **83**, 5174 (1999).
27. The electrostatic kernel corresponds to a cylinder separated by an insulating layer from a horizontal plane. The dielectric constant of the Al_2O_3 layer that was used is 5. The gap of the semiconducting nanotube is taken equal to 0.7 eV as measured with scanning tunneling microscopy on similar material (34).
28. Supplementary data is available at Science Online at www.sciencemag.org/cgi/content/full/1065824/DC1
29. J. Kong, H. Soh, A. M. Cassel, C. F. Quate, H. Dai, *Nature* **395**, 878 (1998).
30. J. Liu *et al.*, *Chem. Phys. Lett.* **303**, 125 (1999).
31. Y. Huang, X. Duan, Q. Wei, C. M. Lieber, *Science* **291**, 630 (2001).
32. P. G. Collins, M. S. Arnold, Ph. Avouris, *Science* **292**, 706 (2001).
33. R. R. Schlittler *et al.*, *Science* **292**, 1136 (2001).
34. L. C. Venema *et al.*, *Phys. Rev. B* **62**, 5238 (2000).
35. F. Léonard, J. Tersoff, *Phys. Rev. Lett.* **84**, 4693 (2000).
36. Four parameters appear in the fit of the model: the thickness d of the Al_2O_3 layer, the difference ΔW between the Au work function and the nanotube ionization potential, the doping fraction f in units of e/atom , and a constant D_0 which describes the dipole resulting from the metal-induced gap states (35). The form of the $I(V_g)$ curve (the width of the gap region and the asymmetry) depends principally on d and ΔW . We obtain $\Delta W = 0.61$ eV, $d = 23$ nm, $f = 0.0015$ and $D_0 = 0.21$ state/(atom-eV). The values of ΔW , f , and D_0 are quite reasonable, but d appears to be overestimated by a factor of around 5. This is likely to originate from an oversimplification of the device geometry, which is used for the description of the Coulomb interaction in the calculation (27).
37. We thank R. E. Smalley for providing the nanotubes, H. W. Ch. Postma and Y. M. Blanter for discussions, E. Swinkels and C. P. Heij for assistance with measurements of the oxide thickness, and B. van den Enden for technical assistance. The research has been supported by the European Community SATURN project and by the Dutch Foundation for Fundamental Research on Material (FOM).

29 August 2001; accepted 26 September 2001
 Published online 4 October 2001;
 10.1126/science.1065824
 Include this information when citing this paper.

European Laboratory for Nonlinear Spectroscopy (LENs), Università di Firenze, and Istituto Nazionale per la Fisica della Materia (INFN), Largo Enrico Fermi 2, 50125 Firenze, Italy.

to inelastic collisions with an initial tiny fraction of Rb atoms in the trapped $|F = 2, m_F = 1\rangle$ state.

In the evolution of the two species during the whole evaporation over 50 s (Fig. 1), the temperature of the K cloud follows that of Rb (Fig. 1A), thus indicating a very efficient interspecies thermalization. It should be noted that once the populations of Rb and K become similar (Fig. 1B), the efficiency of the evaporation decreases: The ratio η between the evaporation threshold and the temperature of the two samples is reduced from about 7 to 5 because of the relative increase of the K heat capacity, which is proportional to the number of atoms, with respect to that of Rb. Even though the evaporation removes only Rb atoms from the trap, the two heat capacities remain comparable in this final stage of evaporation because of relatively large losses of K atoms, and the cooling continues. Such losses are probably due to inelastic collisions within the K sample, which become relevant as the density increases with the lowering of temperature (Fig. 2).

In this crucial phase of the evaporation, the efficiency of the sympathetic cooling process is sustained by the large collisional interaction between the two species. This observation is confirmed by our determination of the elastic K-Rb collisional cross-section in a mixed sample containing a comparable number of atoms of the two species, at a temperature of 13 μ K. Taking advantage of the different trap frequencies for the two species, we have performed a selective parametric excitation of the motion of Rb, recording the subsequent increase of the temperature of the K cloud as a consequence of the collisional energy exchange. From the measured

thermalization rate, using the model presented in (20), we obtain a large value for the zero-energy *s*-wave triplet scattering length, determined to within a sign as $a_{K^{41}\text{-Rb}^{87}} = 206^{+35}_{-38} a_0$ or $a_{K^{41}\text{-Rb}^{87}} = -266^{+55}_{-50} a_0$ (21). These values determine a corresponding range of values for the triplet scattering length of the pair $^{40}\text{K}\text{-}^{87}\text{Rb}$, via mass scaling: We obtain $a_{K^{40}\text{-Rb}^{87}} = -95^{+33}_{-98} a_0$ or $a_{K^{40}\text{-Rb}^{87}} = 30^{+3}_{-2} a_0$, for positive or negative signs of the $^{41}\text{K}\text{-}^{87}\text{Rb}$ scattering length, respectively. At low temperature, the collisional cross-section is proportional to the square of the scattering length (21), and so the two different cases result in completely different scenarios for sympathetic cooling of the fermionic K with Rb.

At the end of the evaporation stage, we observe the formation of a BEC of K out of the thermal sample (22) (Fig. 3). The density of the central part of the K cloud increases as the evaporation threshold is lowered below 40 kHz, indicating the onset of the quantum degeneracy regime. Further evaporation of Rb reduces the number of K atoms in the broad thermal component, which eventually is undetectable, leaving an almost pure condensate. The typical number of atoms in the condensate is $N \approx 10^4$, and a Gaussian fit to the wings of the bimodal density distribution gives a temperature $T \approx 160$ nK (Fig. 4). This observation is consistent with

the theoretical expectation for the transition temperature, $T_C = h/k_B (N v_{ax} v_{rad}^2 / 1.202)^{1/3} = 150$ nK, where h and k_B are the Planck's and Boltzmann's constants (23).

Due to the different gravitational sag of the K and Rb samples in the magnetic trap, their spatial overlap can be reduced at low temperatures. However, we expect the vertical separation of the two clouds to become larger than their thermal radius only below the K critical temperature. As discussed in (24) and confirmed by our experimental observation, this results in a good thermal contact between the two species all the way down to the BEC of K.

We have also measured the K-K triplet scattering length with a conventional cross-dimensional thermalization technique (25), on a pure K sample at 13 μ K, obtaining $a_{K\text{-K}} = 78 \pm 20 a_0$. The repulsive character of the interaction between K atoms (that is, the positive sign of $a_{K\text{-K}}$) results from our observation of stable condensates containing about 10^4 atoms (23). Our direct determination of the scattering length is in agreement with the prediction $a_{K\text{-K}} = 60 \pm 2 a_0$ from molecular photoassociation measurement on the isotope ^{39}K (26).

The K-Rb mixture is an interesting candidate for the formation of ultracold polar molecules, using recently developed schemes

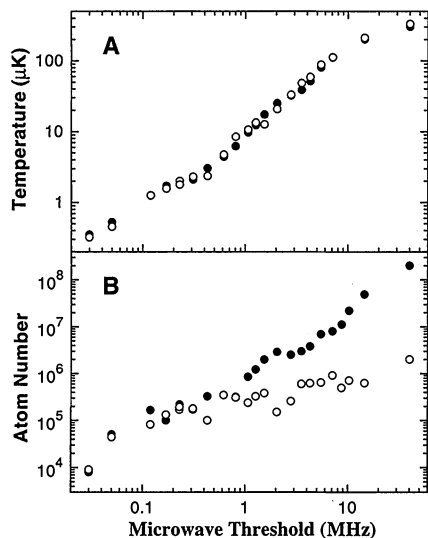


Fig. 1. Evolution of the number of atoms (A) and temperature (B) of the two atomic samples in the magnetic trap as a function of the microwave evaporation threshold of Rb. The solid circles correspond to ^{87}Rb and the open circles to ^{41}K .

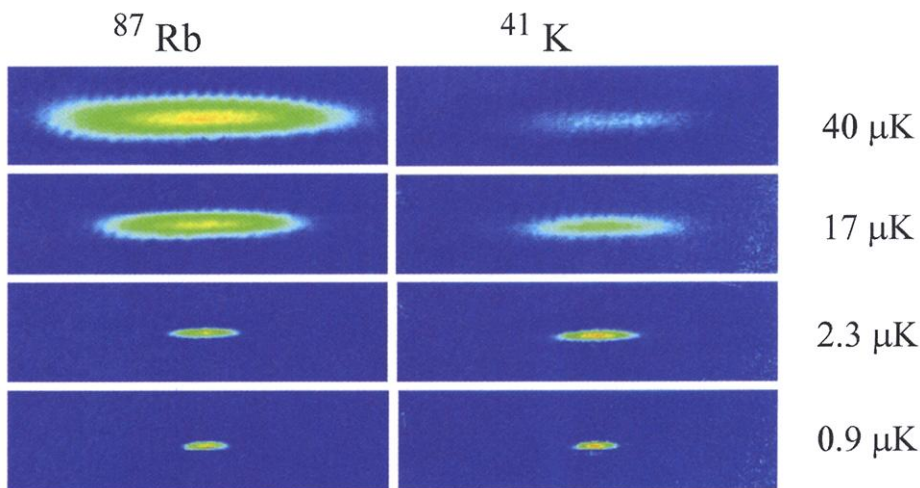
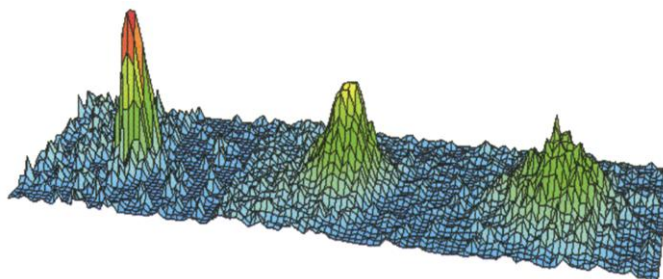


Fig. 2. False color absorption images of Rb (left) and K (right) at four different stages of the sympathetic cooling. The density of the K sample increases by more than two orders of magnitude, going from $4 \times 10^9 \text{ cm}^{-3}$ to $6 \times 10^{11} \text{ cm}^{-3}$, when the temperature is lowered from 40 to 0.9 μ K. The density of the Rb sample is instead approximately constant during the evaporation.

Fig. 3. False color density profiles of the ^{41}K cloud after 15 ms of ballistic expansion, across the phase transition to BEC. From right to left, profiles are as follows: thermal cloud at $T > T_C$; partially condensed sample at $T \approx T_C$; and almost pure condensate at $T < T_C$, containing about 10^4 atoms.



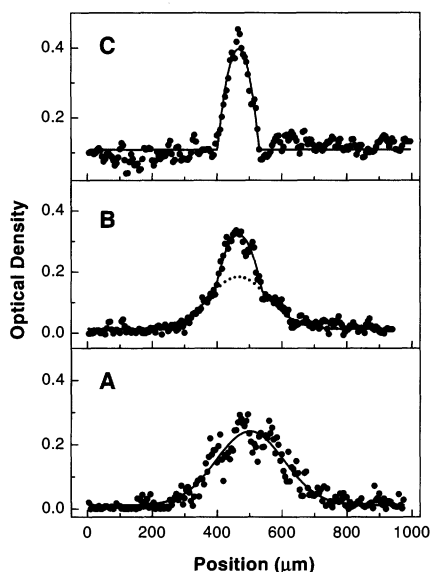


Fig. 4. Density profiles of three samples of ^{41}K after 15 ms of expansion, showing the transition to BEC. (A) Thermal sample at $T = 250$ nK. (B) Mixed sample at $T = 160$ nK. (C) Almost pure condensate. The lines are the best fit with a Gaussian for the thermal component and with an inverted parabola for the condensate component.

(27, 28), which may represent a new system for quantum computing (29).

The possibility of sympathetic cooling to quantum degeneracy with a different species broadens the spectrum of coolable particles to include molecules as well (30). Because Rb is the workhorse for experiments on cold atoms, one could take advantage of recently demonstrated techniques for a simultaneous trapping of the partner species. For example, a BEC of ^{87}Rb has been produced in an optical dipole trap (31), which is an ideal tool to trap a large variety of atoms and molecules lacking a magnetic moment in their ground state. Sympathetic cooling in this kind of trap would have repercussions for high-resolution spectroscopy and metrology (32), tests of fundamental theories (33), and ultracold chemistry.

References and Notes

- M. H. Anderson, J. R. Ensher, M. R. Matthews, C. E. Wieman, E. A. Cornell, *Science* **269**, 198 (1995).
- K. B. Davis *et al.*, *Phys. Rev. Lett.* **75**, 3969 (1995).
- C. C. Bradley, C. A. Sackett, J. J. Tollet, R. G. Hulet, *Phys. Rev. Lett.* **75**, 1687 (1995).
- M. Inguscio, S. Stringari, C. E. Wieman, Eds., *Bose-Einstein Condensation in Atomic Gases*, Proceedings of the International School of Physics "Enrico Fermi," Course CXL (IOS Press, Amsterdam, 1999).
- D. G. Fried *et al.*, *Phys. Rev. Lett.* **81**, 3811 (1998).
- A. Robert *et al.*, *Science* **292**, 461 (2001); published online 22 March 2001 (10.1126/science.1060622).
- S. L. Cornish *et al.*, *Phys. Rev. Lett.* **85**, 1795 (2000).
- M. Prevedelli *et al.*, *Phys. Rev. A* **59**, 886 (1999).
- D. J. Wineland, R. E. Drullinger, F. L. Walls, *Phys. Rev. Lett.* **40**, 1639 (1978).
- C. J. Myatt *et al.*, *Phys. Rev. Lett.* **78**, 586 (1997).
- F. Schreck *et al.*, *Phys. Rev. A* **87**, 011402(R) (2001).
- G. Truscott, K. E. Strecker, W. I. McAlexander, G. B. Partridge, R. G. Hulet, *Science* **291**, 2570 (2001).
- I. Bloch, M. Greiner, O. Mandel, T. W. Hänsch, T. Esslinger, *Phys. Rev. A* **64**, 021402(R) (2001).

- F. S. Cataliotti *et al.*, *Phys. Rev. A* **57**, 1136 (1998).
- B. De Marco, D. S. Jin, *Science* **285**, 1703 (1999).
- F. Schreck *et al.*, *Phys. Rev. Lett.* **87**, 080403 (2001).
- This is a development of the scheme introduced in G. Ferrari, M.-O. Mewes, F. Schreck, C. Salomon, *Opt. Lett.* **24**, 151 (1999).
- A near coincidence between the K ground-state and the Rb excited-state hyperfine splittings induces losses of Rb atoms from the MOTs, when K and Rb lights are injected simultaneously in the TA.
- T. Esslinger, I. Bloch, T. W. Hänsch, *Phys. Rev. A* **58**, R2664 (1998).
- A. Mosk *et al.*, preprint available at <http://xxx.lanl.gov/abs/physics/0107075>.
- The interaction properties of ultracold atoms are described by a single parameter, namely the scattering length a , which we give in atomic units ($a_0 = 0.0529$ nm). The zero-energy collisional cross-section between distinguishable particles can be expressed as $\sigma = 4\pi a^2$. At finite energy, σ depends also on the sign of the scattering length. The mean-field interaction energy in a Bose-Einstein condensate can be expressed as $E = \hbar^2 n a / (\pi M)$, where n is the gas density.
- Because the evaporation ramp is optimized for K, at this stage the Rb sample typically contains less than 10^4 atoms and still follows a thermal distribution. Further reduction of the evaporation threshold results in a complete loss of all the Rb atoms.
- F. Dalfovo, S. Giorgini, L. P. Pitaevskii, S. Stringari, *Rev. Mod. Phys.* **71**, 463 (1999).
- G. Delannoy *et al.*, *Phys. Rev. A* **63**, 051602(R) (2001).
- C. Monroe, E. A. Cornell, C. A. Sackett, C. J. Myatt, C. E. Wieman, *Phys. Rev. Lett.* **70**, 414 (1993).
- H. Wang *et al.*, *Phys. Rev. A* **62**, 052704 (2000).
- A. Fioretti *et al.*, *Phys. Rev. Lett.* **80**, 4402 (1998).
- S. J. J. M. F. Kokkelmans, H. M. J. Vissers, B. J. Verhaar, *Phys. Rev. A* **63**, 031601(R) (2001) and references therein.
- D. DeMille, preprint available at <http://xxx.lanl.gov/abs/quant-ph/0109083>.
- Trapped molecular samples at a few mK have recently been produced [H. L. Bethlem *et al.*, *Nature* **406**, 491 (2000)].
- M. D. Barrett, J. A. Sauer, M. S. Chapman, *Phys. Rev. Lett.* **87**, 010404 (2001).
- C. W. Oates, E. A. Curtis, L. Hollberg, *Opt. Lett.* **25**, 1603 (2000).
- E. A. Hinds, K. Sangster, in *Time Reversal-The Arthur Rich Memorial Symposium*, M. Skalsey, P. H. Bucksbaum, R. S. Conti, D. W. Gidley, Eds. (American Institute of Physics, New York, 1993).
- We benefited from stimulating discussions with all the colleagues of the laser cooling and BEC group at LENS. We thank W. Jastrzebski, N. Poli, F. Riboli, and L. Ricci for their contribution to the experiment; I. Bloch for useful hints for the construction of the magnetic trap; and R. Ballerini, M. DePas, M. Giuntini, A. Hajeb, and A. Orlando for technical assistance. Supported by the Ministero dell'Università e della Ricerca Scientifica; by the European Community under contract HPRICT1999-00111; and by the Istituto Nazionale per la Fisica della Materia, Progetto di Ricerca Avanzata "Photonmatter." G.R. is also at Dipartimento di Fisica, Università di Trento; R.B. is presently at the Department of Physics, University of Dayton, OH; A.S. is also at Dipartimento di Chimica, Università di Perugia; M.I. is also at Dipartimento di Fisica, Università di Firenze.

1 October 2001; accepted 11 October 2001

Published online 18 October 2001;

10.1126/science.1066687

Include this information when citing this paper.

Bulk-Like Features in the Photoemission Spectra of Hydrated Doubly Charged Anion Clusters

Xue-Bin Wang,^{1,2} Xin Yang,^{1,2} John B. Nicholas,³ Lai-Sheng Wang^{1,2*}

We produced gaseous hydrated clusters of sulfate and oxalate anions [$\text{SO}_4^{2-}(\text{H}_2\text{O})_n$ and $\text{C}_2\text{O}_4^{2-}(\text{H}_2\text{O})_n$, where $n = 4$ to 40]. Photoelectron spectra of these clusters revealed that the solute dianions were in the center of the water cluster, $(\text{H}_2\text{O})_n$. For small clusters, these spectra were characteristic of the respective solutes, but beyond the first solvation shell ($n \approx 12$), features in the spectra from the solutes were diminished and a new feature from ionization of water emerged, analogous to bulk aqueous solutions. For large clusters with dimensions greater than 1 nanometer, the solute photoemission features disappeared and the spectra were dominated by the ionization of water as the solvent coverage increased. A smooth transition from gas-phase clusters to behavior of electrolyte solutions was clearly revealed, and the large solvated clusters can be used as molecular models to investigate the photophysics and chemistry of aqueous electrolyte solutions.

Cations often exhibit definitive solvation shells both in bulk aqueous solutions (1, 2) and in water clusters (3) because of their small sizes and strong solute-water interactions. However, the solvation of anions is more complicated, and microscopic informa-

tion about their solvation is relatively limited despite their importance in chemistry and biochemistry (4–6). Most current research on solvated anion clusters has been devoted to the simple halide anions (7–13), with few studies on more complex anions (14–16).